

Isolated prompt photon photoproduction at NLO

M. Fontannaz^a, J. Ph. Guillet^b, G. Heinrich^a

^a*Laboratoire de Physique Théorique¹ LPT,
Université de Paris XI, Bâtiment 210,
F-91405 Orsay, France*

^b*Laboratoire d'Annecy-Le-Vieux de Physique Théorique² LAPTH,
Chemin de Bellevue, B.P. 110, F-74941 Annecy-le-Vieux, France*

Abstract

We present a full next-to-leading order code to calculate the photoproduction of prompt photons. The code is a general purpose program of "partonic event generator" type with large flexibility. We study the possibility to constrain the photon structure functions and comment on isolation issues. A comparison to ZEUS data is also shown.

¹UMR 8627 du CNRS

²UMR 5108 du CNRS, associée à l'Université de Savoie.

1 Introduction

High energy electron-proton scattering at the DESY ep collider HERA is dominated by photoproduction processes, where the electron is scattered at small angles, emitting a quasireal photon which scatters with the proton. These processes are of special interest since they are sensitive to both the partonic structure of the photon as well as of the proton. In particular, they offer the possibility to constrain the (presently poorly known) gluon distributions in the photon, since in a certain kinematical region the subprocess $qg \rightarrow \gamma q$, where the gluon is stemming from a resolved photon, is dominating. Up to now, the experimental errors were too large to discriminate clearly between different sets of gluon distributions in the photon, but a high statistics analysis of the 1996-2000 HERA data on prompt photon photoproduction announced by the ZEUS collaboration will shed new light on this issue.

The calculation of higher order corrections to the Compton process $\gamma q \rightarrow \gamma q$ has been initiated some time ago [1]–[6]. The most recent calculations for prompt photon photoproduction have been done by Gordon/Vogelsang[6] for isolated prompt photon production, Gordon [7] for photon plus jet production and by the group Krawczyk/Zembrzusi [8] for both the inclusive case and γ +jet. However, all of these calculations contain certain drawbacks. In [6], isolation is implemented by adding a subtraction term evaluated in the collinear approximation to the fully inclusive cross section. The programs of [7] and [8] do not contain the full set of NLO corrections. In [7], those parts where the final state photon comes from fragmentation of a hard parton were included only at leading order, arguing that isolation cuts will suppress the fragmentation component in any case to a large extent. Moreover, the box contribution has not been included. In [8], higher order corrections are included only for the case where initial and final state photons are both direct. So not only the contributions from fragmentation, but also the case where the initial photon is resolved are included at Born level only. However, the box contribution has been taken into account.

The calculation presented in this paper takes into account the full NLO corrections to all four subparts. The corresponding matrix elements already have been calculated and tested in previous works [2, 9, 10]. A major advantage of the present code is also given by the fact that it is constructed as a "partonic event generator" and as such is very flexible. Various sorts of observables matching a particular experimental analysis can be defined and histogrammed for an event sample generated once and for all. This strategy already has been applied to construct NLO codes for $\gamma\gamma$ production (DIPHOX) [11] and one or two jets photoproduction [12].

The paper is organized as follows. In section 2 we first describe the theoretical framework and the treatment of the infrared singularities. Then we discuss the implementation of isolation cuts and outline the structure of the code. Section 3 is devoted to phenomenology. We study the effect of isolation, determine the kinematic region which is most sensitive to the gluon distribution in the photon and illustrate the sensitivity of the cross section to the energy of the incoming photon. We give results for inclusive isolated prompt photon production and compare with a recent analysis of ZEUS data [13], before we come to the conclusions in section 4.

2 Theoretical formalism and description of the method

In this section the general framework for prompt photon photoproduction will be outlined. We will review the contributing subprocesses, the treatment of infrared singularities and the implementation of isolation cuts.

2.1 The subprocesses contributing at NLO

The inclusive cross section for $ep \rightarrow \gamma X$ can symbolically be written as a convolution of the parton densities of the incident particles (resp. fragmentation function for an outgoing parton fragmenting into a photon) with the partonic cross section $\hat{\sigma}$

$$d\sigma^{ep \rightarrow \gamma X}(P_p, P_e, P_\gamma) = \sum_{a,b,c} \int dx_e \int dx_p \int dz F_{a/e}(x_e, M) F_{b/p}(x_p, M_p) d\hat{\sigma}^{ab \rightarrow cX}(x_p P_p, x_e P_e, P_\gamma/z, \mu, M, M_p, M_F) D_{\gamma/c}(z, M_F) \quad (1)$$

where M, M_p are the initial state factorization scales, M_F the final state factorization scale and μ the renormalization scale.

The subprocesses contributing to the partonic reaction $ab \rightarrow cX$ can be divided into four categories which will be denoted by 1. direct direct 2. direct fragmentation 3. resolved direct 4. resolved fragmentation. The cases "direct direct" and "resolved direct" correspond to $c = \gamma$ and $D_{\gamma/c}(z, M_F) = \delta_{c\gamma} \delta(1-z)$ in (1), that is, the prompt³ photon is produced directly in the hard subprocess. The cases with "direct" attributed to the initial state photon correspond to $a = \gamma$, with $F_{\gamma/e}$ approximated by the Weizsäcker-Williams formula for the spectrum of the quasisreal photons

$$f_\gamma^e(y) = \frac{\alpha_{em}}{2\pi} \left\{ \frac{1 + (1-y)^2}{y} \ln \frac{Q_{\max}^2(1-y)}{m_e^2 y^2} - \frac{2(1-y)}{y} \right\}. \quad (2)$$

The "resolved" contributions are characterized by a resolved photon in the initial state where a parton stemming from the photon instead of the photon itself participates in the hard subprocess. In these cases, $F_{a/e}(x_e, M)$ is given by a convolution of the Weizsäcker-Williams spectrum with the parton distributions in the photon:

$$F_{a/e}(x_e, M) = \int_0^1 dy dx_\gamma f_\gamma^e(y) F_{a/\gamma}(x_\gamma, M) \delta(x_\gamma y - x_e) \quad (3)$$

Examples of diagrams contributing at Born level to the four categories above are shown in Figs. 1 and 2.

In the case of the "direct direct" part, only the Compton process $\gamma q \rightarrow \gamma q$ contributes at leading order, at NLO the $\mathcal{O}(\alpha_s)$ corrections from $\gamma q \rightarrow \gamma qg$ resp. $\gamma g \rightarrow \gamma q\bar{q}$ and the corresponding virtual corrections contribute. We also included the box contribution (Fig. 3) into the "direct direct" part since it is known to be sizeable [4], although it is formally a NNLO contribution.

In the "direct fragmentation" part, the final state photon comes from the fragmentation of a hard parton participating in the short distance subprocess. From a technical point of view, a final state quark-photon collinear singularity appears in the calculation of the subprocess $\gamma g \rightarrow \gamma q\bar{q}$. At higher orders, final state multiple collinear singularities appear in any subprocess where a high p_T parton (quark or gluon) undergoes a cascade of successive collinear splittings ending up with a quark-photon splitting. These singularities are factorized to all orders in α_s and absorbed, at some arbitrary fragmentation scale M_F , into quark and gluon fragmentation functions to a photon, $D_{\gamma/c}(z, M_F^2)$. When the fragmentation scale M_F , chosen of the order of the hard scale of the subprocess, is large compared to any typical hadronic scale ~ 1 GeV, these functions behave roughly as $\alpha/\alpha_s(M_F^2)$. Then a power counting argument tells that these fragmentation contributions are asymptotically of the same order in α_s as the Born term. A consistent NLO calculation thus requires the inclusion of the $\mathcal{O}(\alpha_s)$ corrections to these contributions.

Note that the singularity appearing in the process $\gamma g \rightarrow \gamma q\bar{q}$ when the final state photon is emitted by the quark and becomes collinear, is subtracted and absorbed by the fragmentation function at the scale M_F , as explained above. Therefore both the "direct direct" and the "direct fragmentation" parts *separately* depend strongly on M_F and the attribution of the finite terms to either of these parts is scheme dependent. Only in the sum of these parts the M_F dependence flattens as expected.

The collinear singularities appearing at NLO if the *incident* photon splits into a collinear $q\bar{q}$ pair are absorbed into the functions $F_{q/\gamma}(x_\gamma, M)$ at the factorization scale M . (Analogous for the

³By "prompt" we mean that the photon is not produced from the decay of light mesons.

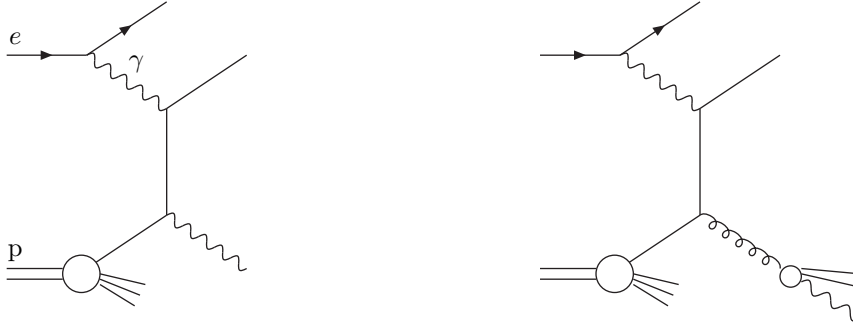


Figure 1: Examples of direct direct and direct fragmentation contributions at leading order

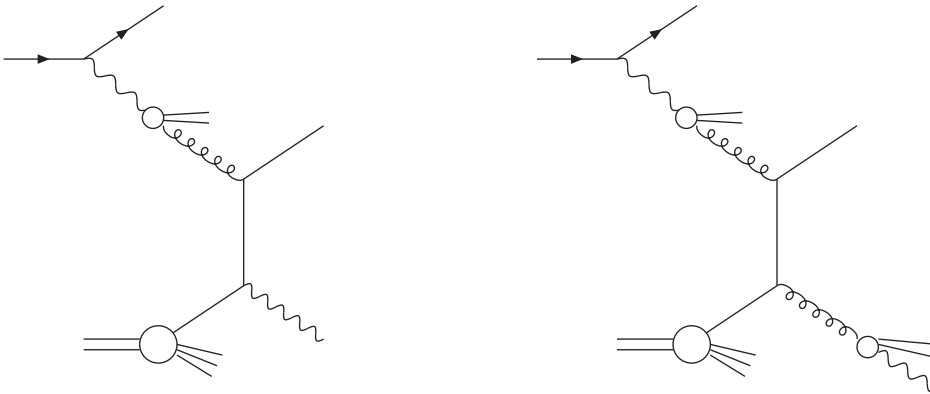


Figure 2: Examples of resolved direct and resolved fragmentation contributions at leading order

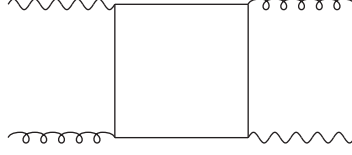


Figure 3: The box contribution

proton distribution functions $F_{b/p}(x_p, M_p)$; we will set $M_p = M$ in the following.) Thus, by the same reasoning as above for the final state, the "initial direct" and "initial resolved" parts separately show a strong dependence on M which cancels out in the sum. Therefore it has to be stressed that only the sum over all four parts has a physical meaning. Figure 5 illustrates these cancellation mechanisms.

The overall reduction of the scale dependence when going from leading to next-to-leading order can be seen in Fig. 4. The scales M_F and M have been set equal to μ , and μ has been varied between $\mu = p_T^\gamma/2$ and $\mu = 2p_T^\gamma$. One can see that the NLO cross section is much more stable against scale variations, it varies by less than 10% in this μ range.

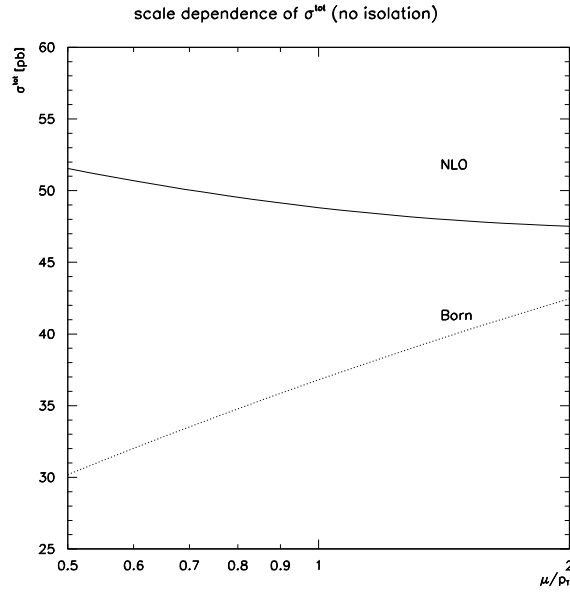


Figure 4: Dependence of the total cross section on scale variations. $\mu = M = M_F$ is varied between $\mu = p_T^\gamma/2$ and $\mu = 2p_T^\gamma$.

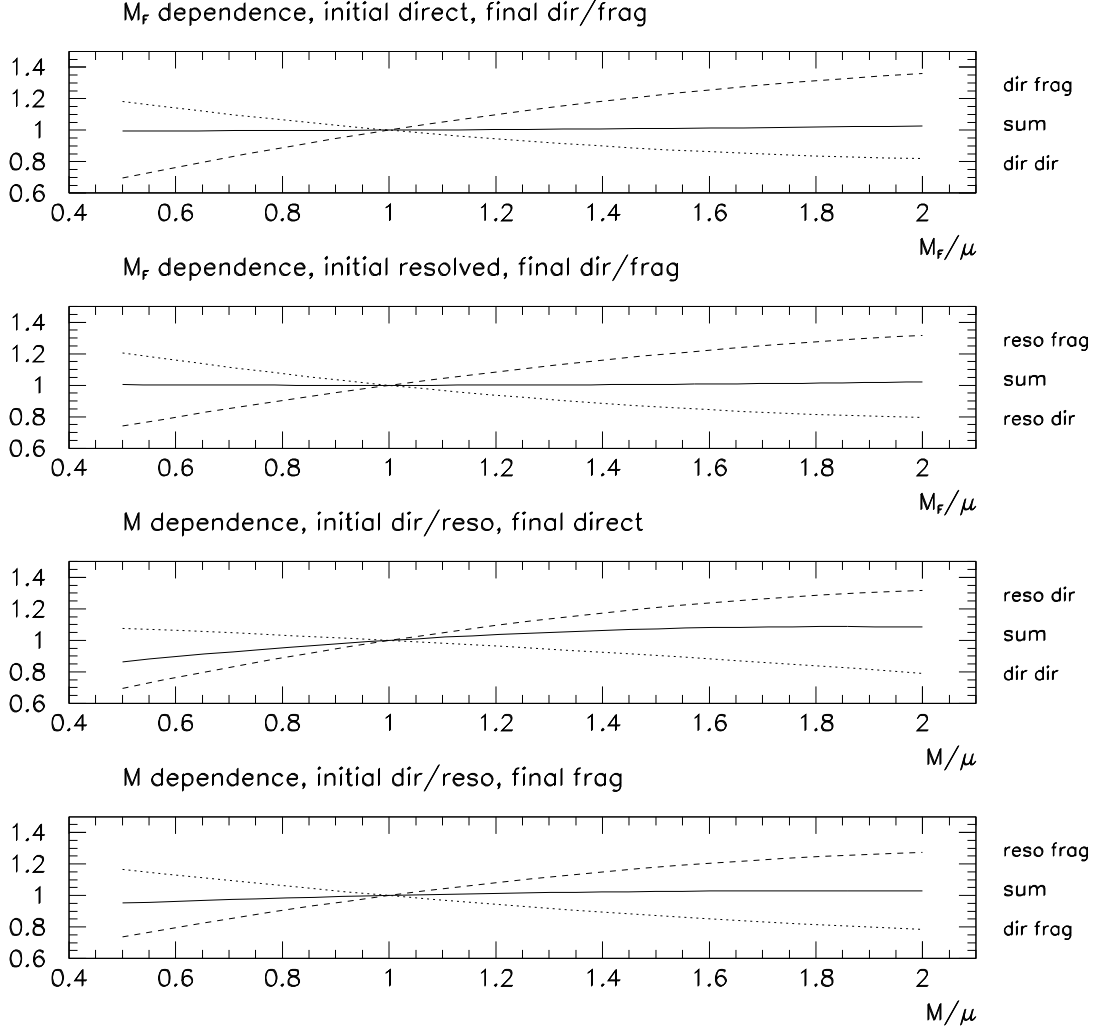


Figure 5: Cancellation of the leading dependence on the fragmentation scale M_F between contributions from direct and fragmentation final states, and on the factorization scale M between parts with direct and resolved initial state. The results are normalized to the total cross section at $M_F = M = \mu = p_T^\gamma$.

2.2 Treatment of infrared singularities

There are basically two methods to isolate the infrared singularities appearing in the calculation at NLO: The phase space slicing method [15] and the subtraction method [16]. The method used here follows the approach of [11, 14] which combines these two techniques. We will outline the strategy only shortly, for more details we refer to [11].

For a generic reaction $1 + 2 \rightarrow 3 + 4 + 5$, at least two particles of the final state, say 3 and 4, have a high p_T and are well separated in phase space, while the last one, say 5, can be soft, and/or collinear to either of the four others. In order to extract these singularities, the phase space is cut into two regions:

- part I where the norm p_{T5} of the transverse momentum of particle 5 is required to be less than some arbitrary value p_{Tm} taken to be small compared to the other transverse momenta. This cylinder contains the infrared and the initial state collinear singularities. It also contains a small fraction of the final state collinear singularities.
- parts II a(b) where the transverse momentum vector of the particle 5 is required to have a norm larger than p_{Tm} , and to belong to a cone $C_3(C_4)$ about the direction of particle 3(4), defined by $(\eta_5 - \eta_i)^2 + (\phi_5 - \phi_i)^2 \leq R_{th}^2$ ($i = 3, 4$), with R_{th} some small arbitrary number. $C_3(C_4)$ contains the final state collinear singularities appearing when 5 is collinear to 3(4).
- part II c where p_{T5} is required to have a norm larger than p_{Tm} , and to belong to neither of the two cones C_3, C_4 . This slice yields no divergence, and can thus be treated directly in 4 dimensions.

The contributions from regions I and IIa,b are calculated analytically in $d = 4 - 2\epsilon$ dimensions and then combined with the corresponding virtual corrections such that the infrared singularities cancel, except for the initial (resp. final) state collinear singularities, which are factorized and absorbed into the parton distribution (resp. fragmentation) functions.

After the cancellation, the finite remainders of the soft and collinear contributions in parts I and II a,b,c separately depend on large logarithms $\ln p_{Tm}$, $\ln^2 p_{Tm}$ and $\ln R_{th}$. When combining the different parts, the following cancellations of the p_{Tm} and R_{th} dependences occur:

In part I, the finite terms are approximated by collecting all the terms depending logarithmically on p_{Tm} and neglecting the terms proportional to powers of p_{Tm} . On the contrary, the R_{th} dependence in the conical parts II a and II b, is kept exactly. This means that an exact cancellation of the dependence on the unphysical parameter R_{th} between part II c and parts II a,b occurs, whereas the cancellation of the unphysical parameter p_{Tm} between parts II c, II a,b and part I is only approximate. The parameter p_{Tm} must be chosen small enough with respect to p_T^γ in order that the neglected terms can be safely dropped out. On the other hand, it cannot be chosen too small since otherwise numerical instabilities occur. We have investigated the stability of the cross section by varying p_{Tm} and R_{th} between 0.005 and 0.1 (see Figure 6) and accordingly chosen the optimal values $p_{Tm} = 0.05 \text{ GeV}$, $R_{th} = 0.05$.

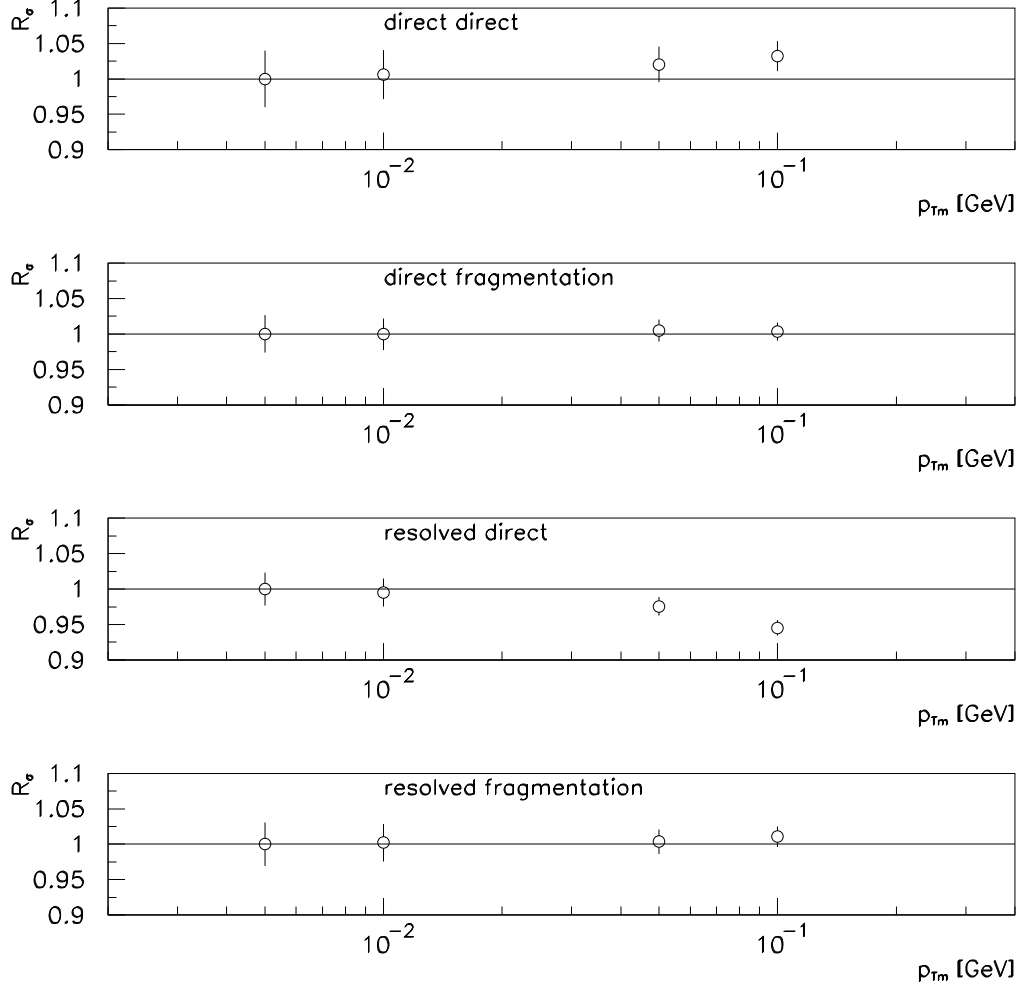


Figure 6: Dependence of the total cross section on variations of the slicing parameter p_{Tm} . R_σ denotes the total (nonisolated) cross section normalized to the total cross section evaluated with $p_{Tm} = 0.005$, $R_\sigma(p_{Tm}) = \sigma^{tot}(p_{Tm})/\sigma^{tot}(p_{Tm} = 0.005)$. One can see that there is a plateau where the cross section is fairly insensitive to variations of p_{Tm} . The same study has been made for the dependence on R_{th} , but there the cross section is completely stable within the numerical errors since the R_{th} dependence has been kept exactly in all parts of the matrix element.

2.3 Implementation of isolation cuts

In order to single out the prompt photon events from the huge background of secondary photons produced by the decays of π^0, η, ω mesons, isolation cuts have to be imposed on the photon signals in the experiment. A commonly used isolation criterion is the following⁴: A photon is isolated if, inside a cone centered around the photon direction in the rapidity and azimuthal angle plane, the amount of hadronic transverse energy E_T^{had} deposited is smaller than some value $E_{T\,max}$ fixed by the experiment:

$$\left. \begin{aligned} (\eta - \eta_\gamma)^2 + (\phi - \phi_\gamma)^2 &\leq R_{\text{exp}}^2 \\ E_T^{had} &\leq E_{T\,max} \end{aligned} \right\} \quad (4)$$

Following the conventions of the ZEUS collaboration, we used $E_{T\,max} = \epsilon p_T^\gamma$ with $\epsilon = 0.1$ and $R_{\text{exp}} = 1$. Isolation not only reduces the background from secondary photons, but also substantially reduces the fragmentation components, as will be illustrated in section 3.1.

Furthermore, it is important to note that the isolation parameters must be carefully fixed in order to allow a comparison between data and perturbative QCD calculations. Indeed a part of the hadronic energy measured in the cone may come from the underlying event; therefore even the direct contribution can be cut by the isolation condition if the latter is too stringent. Let us estimate the importance of this effect and assume that the underlying event one-particle inclusive distribution is given by

$$\frac{dn^{(1)}}{p_T dp_T d\eta d\phi} = \frac{\bar{n}}{2\pi} \frac{4}{\langle p_T \rangle^2} e^{-\frac{2p_T}{\langle p_T \rangle}}, \quad (5)$$

$n^{(1)}$ being normalized to \bar{n} particles per unit of rapidity. The probability that the isolation condition is fulfilled by a particle from an underlying event is

$$\begin{aligned} n_{isol}^{(1)} &= \int_{cone} d\phi d\eta \int_{E_{T\,max}}^{\infty} p_T dp_T \frac{dn^{(1)}}{p_T dp_T d\eta d\phi} \\ &= R_{\text{exp}}^2 \frac{\bar{n}}{2} \left(1 + \frac{2E_{T\,max}}{\langle p_T \rangle} \right) e^{-\frac{2E_{T\,max}}{\langle p_T \rangle}} \end{aligned} \quad (6)$$

With the ZEUS isolation parameters, $E_{T\,max} = 0.5 \text{ GeV}$ for a photon of $p_T^\gamma = 5 \text{ GeV}$. Using $\bar{n} = 3$ and $\langle p_T \rangle \approx 0.35 \text{ GeV}$ extracted from [18], one obtains

$$n_{isol}^{(1)} \approx 0.33$$

This estimation is very rough and underestimates the true effect because there is also a non-negligible probability to fulfill the isolation condition with two underlying particles falling into the cone. Only a detailed Monte Carlo description of the underlying events can allow a reliable estimate of this non-perturbative effect. Here we just note that the cut put by ZEUS ($E_{T\,max} \approx 0.5 \text{ GeV}$) is likely to be too low to eliminate any underlying event contamination and therefore makes a comparison between the partonic level QCD predictions and the (hadronic level) data difficult.

2.4 Features of the code

The code consists of four subparts corresponding to each of the four categories of subprocesses. For each category, the functions corresponding to the parts I, II a,b,c described in section 2.2 are integrated separately with the numerical integration package BASES[23]. Based on the grid produced by this integration, partonic events are generated with SPRING[23] and stored into an NTUPLE or histogrammed directly. It has to be emphasized that we generate final state *partonic* configurations.

⁴ A more sophisticated criterion has been proposed in [17], in which the veto on accompanying hadronic transverse energy is the more severe, the closer the corresponding hadron to the photon direction. It has been designed to make the “fragmentation” contribution vanish in an infrared safe way.

Hence this type of program does not provide an exclusive portrait of final states as given by hadronic event generators like PYTHIA or HERWIG. On the other hand, the latter are only of some improved leading logarithmic accuracy. The information stored in the NTUPLE are the 4-momenta of the outgoing particles, their types (i.e. quark, gluon or photon), the energy of the incident photon and, in the fragmentation cases, the longitudinal fragmentation variable associated with the photon from fragmentation. Furthermore a label is stored that allows to identify the origin of the event, e.g. if it comes from a $2 \rightarrow 2$ or a $2 \rightarrow 3$ process. Based on the information contained in these NTUPLES, suitable observables can be defined and different jet algorithms can be studied. The isolation cuts are included already at the integration level, but the user of the program can turn isolation on or off and vary the input parameters for the isolation cut at will.

3 Numerical results and comparison to ZEUS data

In this section we present some numerical results for isolated prompt photon production. We restrict ourselves to the inclusive case, photon + jet production will be discussed in detail in a forthcoming publication.

For the parton distributions in the proton we take the MRST2 [19] parametrization. Our default choice for the photon distribution functions is AFG [20], for comparisons we also used the GRV [21] distributions transformed to the $\overline{\text{MS}}$ scheme. For the fragmentation functions we use the parametrization of Bourhis et al [22]. We take $n_f = 4$ flavors, the contributions from the b quark can be neglected since the typical energy scale of the partonic process is too close to the b -production threshold. For $\alpha_s(\mu)$ we use an exact solution of the two-loop renormalization group equation, and not an expansion in $\log(\mu/\Lambda)$. Unless stated otherwise, the scale choices $M = M_F = \mu = p_T^\gamma$ have been used. The rapidities refer to the ep laboratory frame, with the HERA convention that the proton is moving towards positive rapidity. HERA operates with an electron energy of 27.5 GeV and a proton energy of 820 GeV.

Following the ZEUS collaboration [13], the parameters for the Weizsäcker-Williams spectrum are $Q_{\text{max}}^2 = 1 \text{ GeV}^2$ and the photon energy $y = E_\gamma/E_e$ has been restricted to the range $0.2 < y < 0.9$. Note that experimentally, the energy of the incoming photon in photoproduction processes is reconstructed from the final hadron energies with the Jacquet-Blondel method,

$$y_{JB} = \frac{\sum(E - p_z)}{2E_e} \quad (7)$$

where the sum is over all calorimeter cells, E is the energy deposited in the cell and $p_z = E \cos \theta$. In order to obtain the "true" photon energy y , corrections for detector effects and energy calibration have to be applied to y_{JB} . These corrections are assumed to be uniform over the whole y range and enter into the experimental systematic error. However, as the background varies with the photon energy y , these corrections may not be uniform. It has to be emphasized that the cross section is very sensitive to a variation of the energy range of the photon. (See Figure 12 and discussion below.)

3.1 Numerical results for inclusive prompt photon production

If not stated otherwise, all plots showing the photon rapidity (η^γ) dependence are integrated over $5 \text{ GeV} < p_T^\gamma < 10 \text{ GeV}$ and $0.2 < y = E_\gamma/E_e < 0.9$.

Figure 7 shows a comparison of the NLO to the leading order result for the isolated cross section $d\sigma/d\eta^\gamma$. The importance of the box contribution is clearly visible. The higher order corrections enhance the isolated cross section by about 40%.

Fig. 8 shows the rapidity distribution of the full cross section before and after isolation. As already mentioned in section 2.3, we used the isolation cuts $E_{T\text{max}} = \epsilon p_T^\gamma$ with $\epsilon = 0.1$ and $R_{\text{exp}} = 1$ to match those of the ZEUS collaboration. Fig. 8 also shows the effect of isolation on the

fragmentation part⁵ separately. Isolation reduces the fragmentation component to about 6% of the total isolated cross section.

In Fig. 9 the relative magnitude of all four components contributing to $d\sigma^{ep\rightarrow\gamma X}/d\eta^\gamma$ before and after isolation is shown. Note that isolation *increases* the contributions with a direct photon in the final state slightly since there the cut mainly acts on a negative term, which is the one where parton 5 is collinear to the photon. It should be emphasized that Figure 9 has to be read with care since the individual parts have no physical meaning and are very sensitive to scale changes. Nevertheless the dominance of the resolved direct part remains if we choose e.g. $\mu = M = M_F = p_T^\gamma/2$ or $2p_T^\gamma$.

Figure 10 shows the relative magnitude of contributions from resolved and direct photons in the initial state to the isolated cross section. From the p_T^γ distribution one can conclude that the resolved part dominates the cross section for small values of p_T^γ such that it would be useful to look at the photon rapidity distribution at $p_T^\gamma = 5$ GeV in order to discriminate between different parton distribution functions in the photon.

Since the *gluon* distribution in the photon is of particular interest, the sensitivity to the gluon in the photon is investigated in Fig. 11. One can see that the gluon distribution in the photon starts to become sizeable only for photon rapidities $\eta^\gamma > 1$ and dominates over the quark distribution for about $\eta^\gamma > 2.5$. Therefore the region of large photon rapidities and small photon p_T is the one where the sensitivity to the gluon in the photon is largest. In order to test further the sensitivity to the gluon, we increased the gluon distribution in the photon uniformly by 20%. As can be anticipated from Fig. 11, the effect becomes sizeable only for $\eta^\gamma > 2$ and leads to an increase of the cross section by about 10% for $\eta^\gamma > 2.5$. We conclude that in the region $\eta^\gamma < 1$, there is basically no sensitivity to the gluon in the photon. However, investigating the photon + jet cross section instead of the inclusive case offers larger possibilities to constrain the gluon in the photon since there one can vary the photon *and* the jet rapidities in order to single out a kinematic region where the sensitivity is large [24].

Figure 12 shows the effect of a ten percent uncertainty in the "true" bounds of the photon energy y . One can see that a change of the lower bound on y has a large effect, in particular at large photon rapidities. This comes from the fact that the Weizsäcker-Williams distribution is large and steeply falling at small y . Increasing the lower bound on y therefore removes a large fraction of the direct events with lower energy initial photons. ($y = x_e$ for the direct events and large η^γ correspond to small x_e .) At large photon rapidities the spread due to the use of different parton distribution functions for the photon is smaller than the one caused by a 10% variation of the lower bound on y . On the other hand, the region of large photon rapidities is of special interest since there the gluon in the photon is dominating. Therefore a small experimental error in the reconstruction of the "true" photon energy is crucial in order to be able to discriminate between different sets of parton distribution functions in the photon.

It has been tested that the effect of using different *proton* distribution functions – for example the CTEQ4M or the MRST1 set of proton distribution functions – is of the order of 3% at most. In all photon rapidity bins the spread is smaller than the one caused by different sets of photon distribution functions (which is about 10% at small photon rapidities, see e.g. Fig. 14). Thus a discrimination between different sets of photon distribution functions should be possible with the forthcoming full 1996-2000 data set analysis, where the errors on the data are expected to be small enough.

⁵By "fragmentation part" we mean the sum of the two subparts "direct fragmentation" and "resolved fragmentation". Analogously, "resolved" denotes the sum of "resolved direct" and "resolved fragmentation".

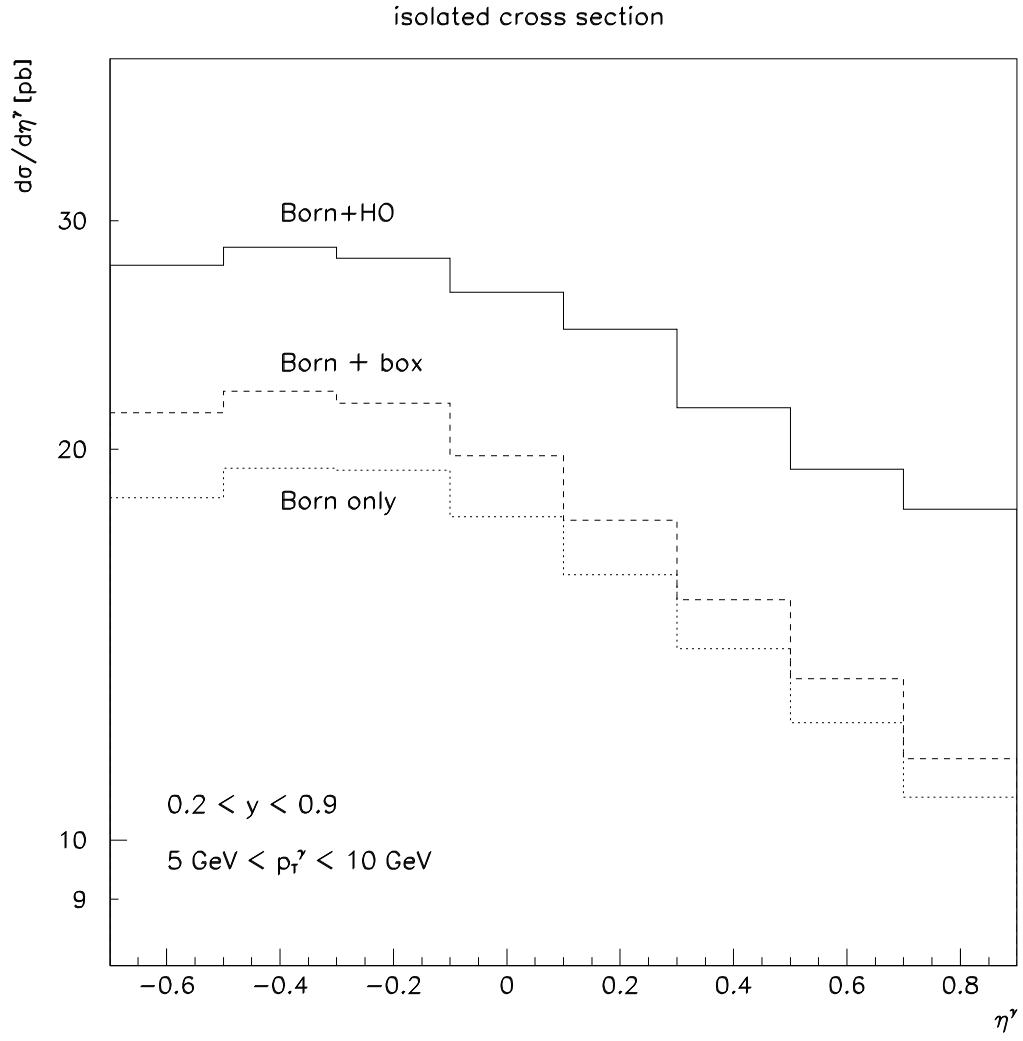


Figure 7: Comparison of NLO to LO result for the photon rapidity distribution.

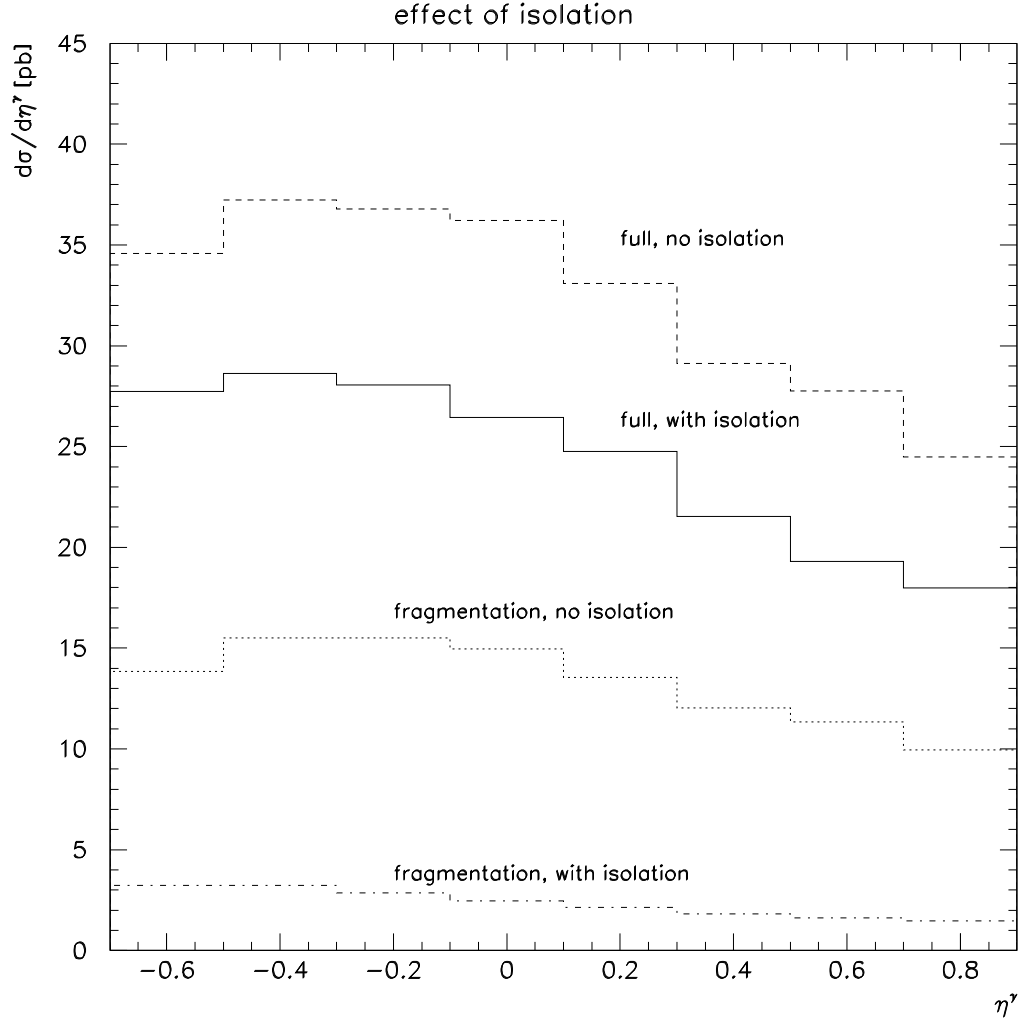


Figure 8: Effect of isolation on the photon rapidity distribution $d\sigma^{ep \rightarrow \gamma X}/d\eta^\gamma$ for the full cross section and for the fragmentation components separately. Isolation with $\epsilon = 0.1$, $R_{\text{exp}} = 1$.

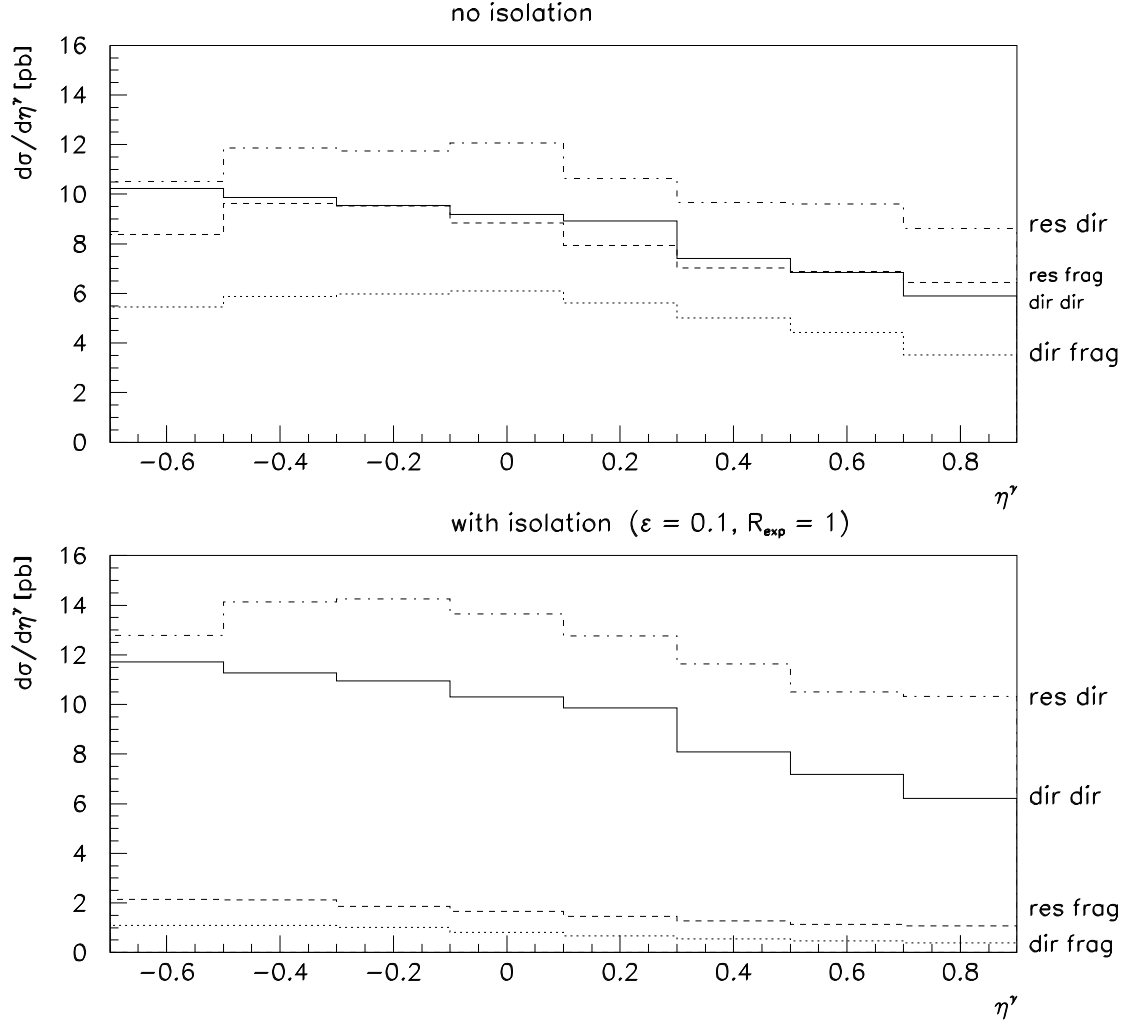


Figure 9: Relative magnitude of all four components contributing to $d\sigma^{ep \rightarrow \gamma X}/d\eta^\gamma$ for the scale choice $\mu = M = M_F = p_T^\gamma$.

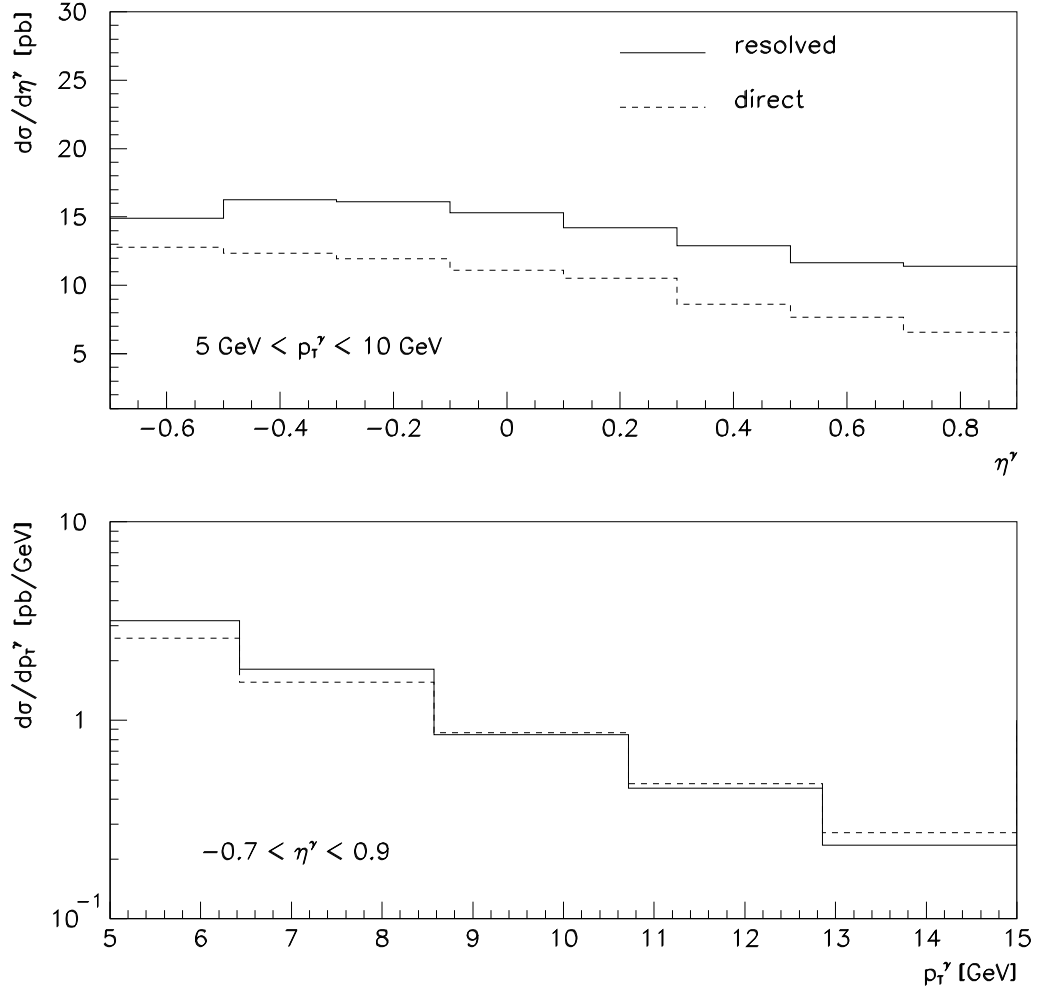


Figure 10: Comparison of contributions from resolved and direct photons in the initial state for the photon rapidity and transverse momentum distribution, with isolation.

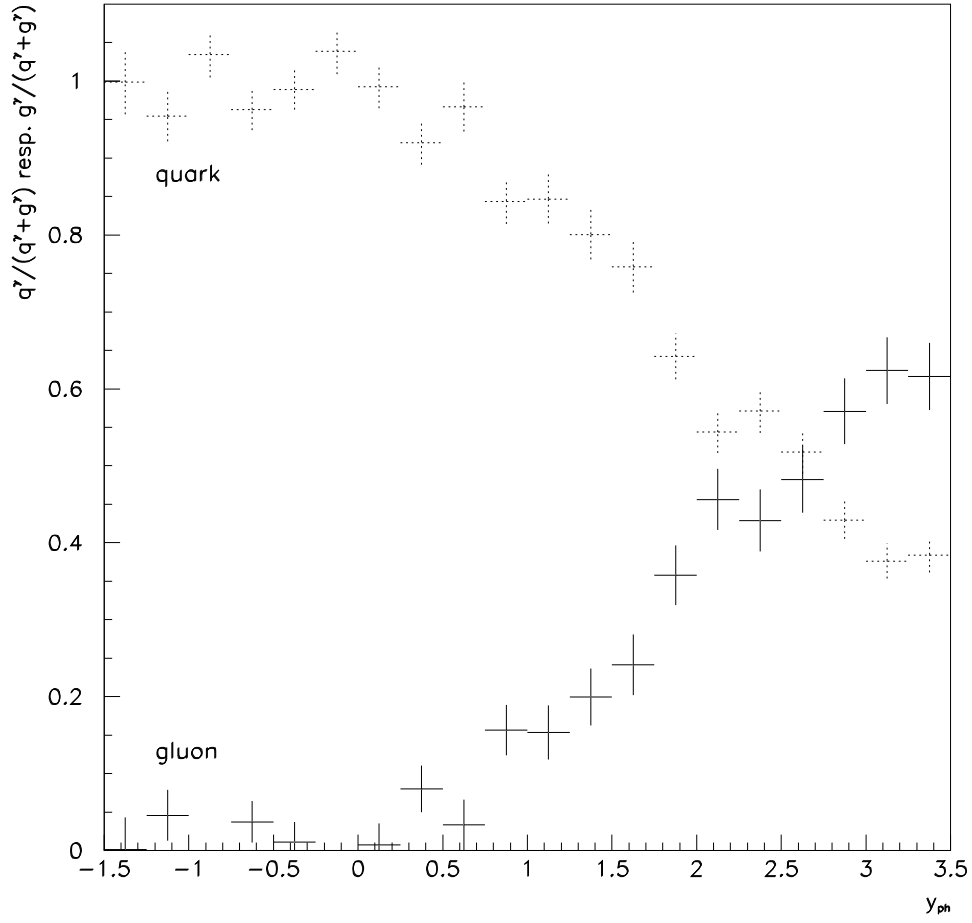


Figure 11: Ratio of the contribution from quark resp. gluon distributions in the photon to the full resolved part.

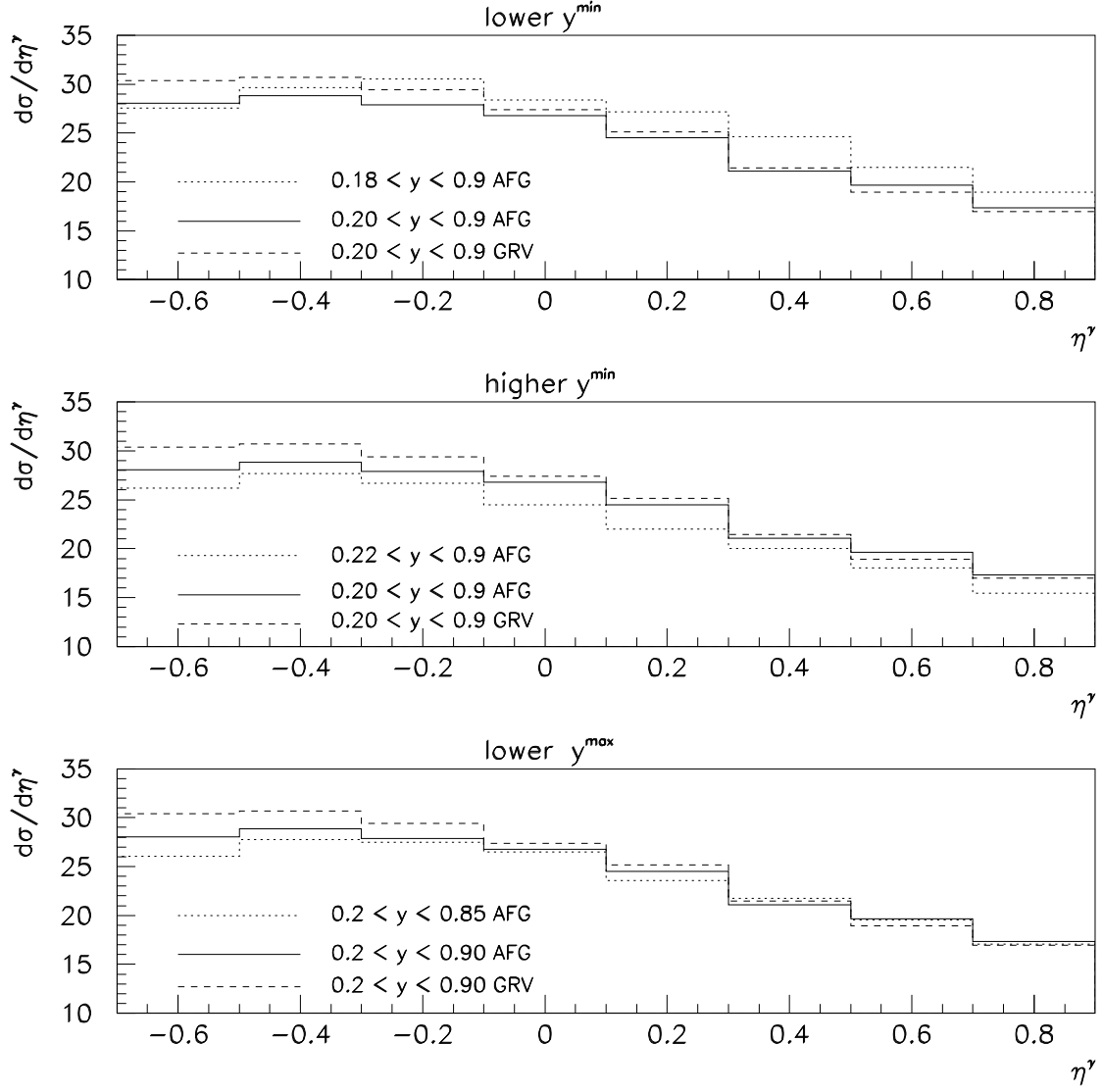


Figure 12: Photon rapidity distribution $d\sigma^{ep \rightarrow \gamma X}/d\eta^\gamma$ for isolated prompt photons integrated over $5 \text{ GeV} < p_T^\gamma < 10 \text{ GeV}$ and different lower bounds on y . Solid line: $0.2 < y < 0.9$ with AFG photon structure functions, dotted line: bounds on y changed by about 10%, dashed line: $0.2 < y < 0.9$ with GRV photon structure functions

3.2 Comparison with ZEUS data

In this section we compare our results to the ZEUS 1996-97 data on inclusive prompt photon photoproduction [13]. Figures 13 and 14 show the photon p_T and rapidity distributions with AFG resp. GRV sets of structure functions for the photon. For the p_T distribution the agreement between data and theory is quite good. In the rapidity distribution (Fig. 14) the data fluctuate a lot, such that the agreement is still satisfactory. However, it seems that theory underpredicts the data in the backward region, whereas the theoretical prediction tends to be higher at large photon rapidities. The curves of Gordon [7] and Krawczyk/Zembrzusi [8] given in [13] also show this trend. At high η^γ the reason for the difference could be that the isolation cut in the experiment removes more events than in the theoretical (parton level) simulation, as discussed in section 2.3.

Figure 15 shows that the discrepancy between theory and data at low η^γ comes mainly from the domain of small photon energies, whereas the discrepancy at large η^γ is only present in the range of large photon energies. Note that at large η^γ and large y the resolved part dominates and the underlying event could have a large multiplicity. Therefore the isolation criterion could also cut on the non-fragmentation contributions as discussed in section 2.3.

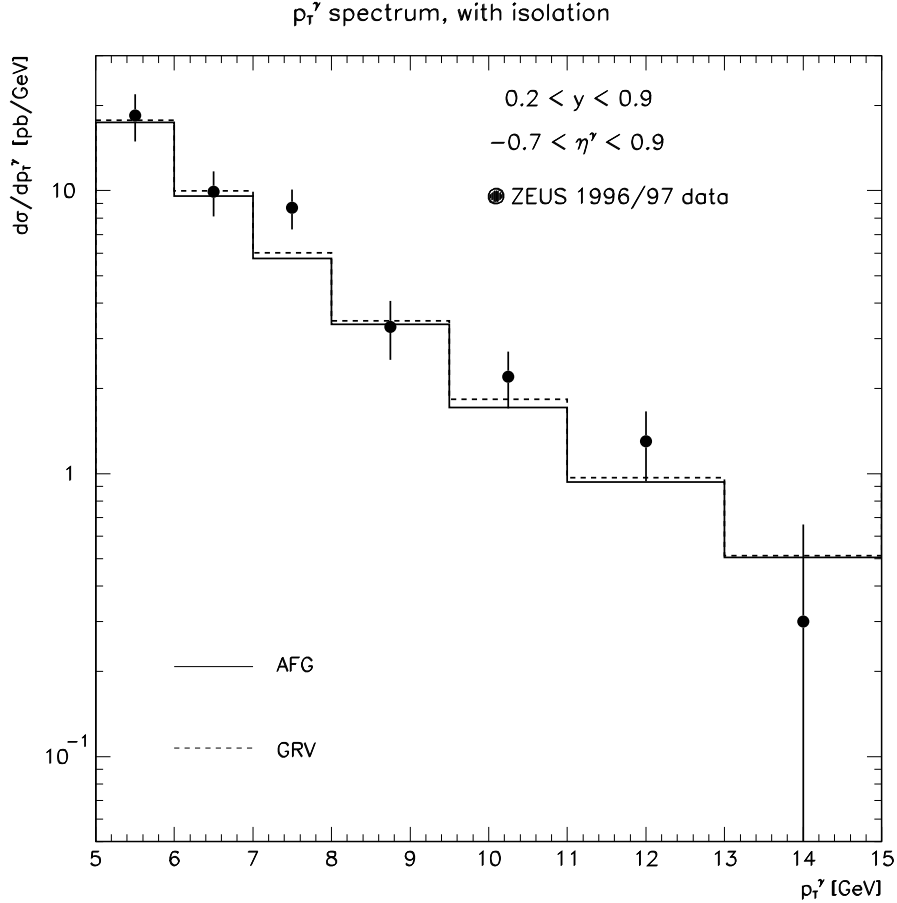


Figure 13: Comparison to ZEUS data of photon p_T distribution $d\sigma^{ep \rightarrow \gamma X}/dp_T^\gamma$ for isolated prompt photons. Results for two different sets of parton distributions in the photon are shown.

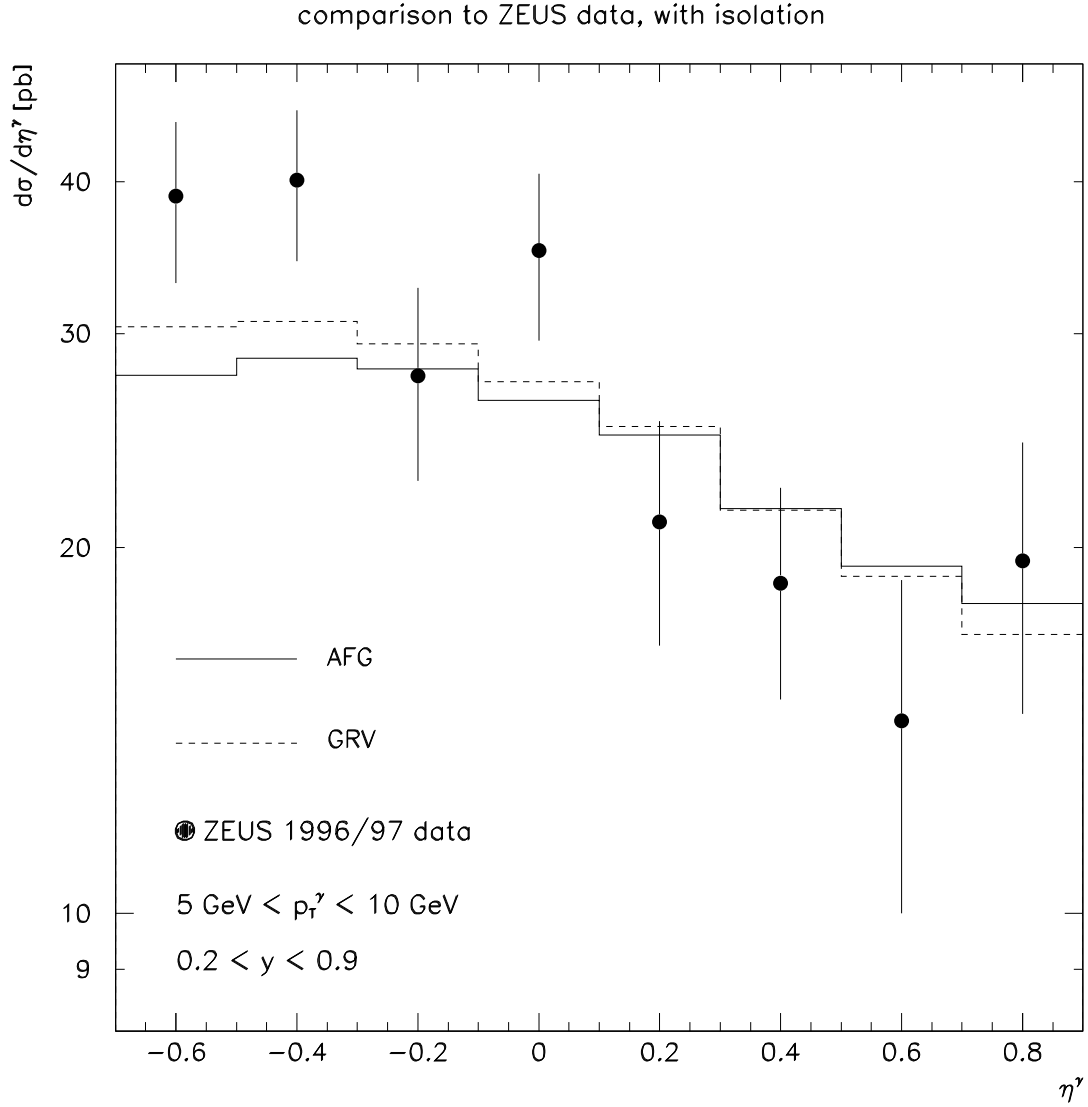


Figure 14: Comparison to ZEUS data of photon rapidity distribution $d\sigma^{ep \rightarrow \gamma X}/d\eta^\gamma$ for isolated prompt photons.

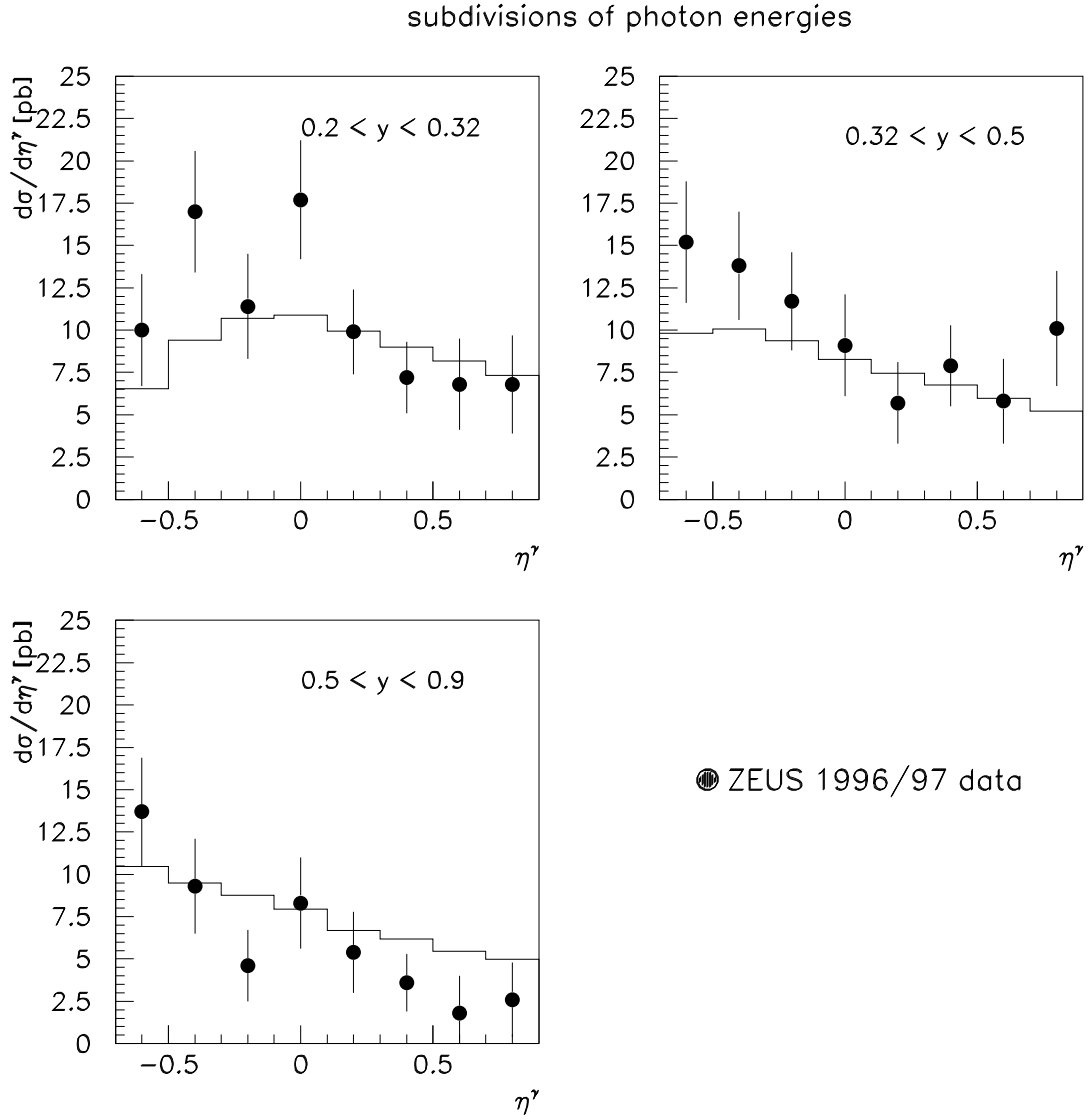


Figure 15: Photon rapidity distribution $d\sigma^{ep \rightarrow \gamma X}/d\eta^\gamma$ integrated over $5 \text{ GeV} < p_T^\gamma < 10 \text{ GeV}$ and different subdivisions of photon energies: (a) $0.2 < y < 0.32$, (b) $0.32 < y < 0.5$, (c) $0.5 < y < 0.9$.

4 Conclusions

We have presented a program for prompt photon photoproduction which includes the full next-to-leading order corrections to all contributing subparts. It is a general purpose code of partonic event generator type and as such very flexible.

We used it to study the possibility to constrain the quark and gluon distributions in the photon. It turned out that the sensitivity to the *gluon* distribution in the photon is negligible in the rapidity range $-0.7 < \eta^\gamma < 0.9$ studied by ZEUS.

A discrimination between the AFG/GRV sets of parton distributions in the photon is not possible with the present experimental errors on the ZEUS 1996/97 data. However, a forthcoming analysis of all 1996-2000 data announced by the ZEUS collaboration will drastically improve this situation.

We have shown that the cross section is very sensitive to small variations of the photon energy range. Therefore a good control of the experimental error on the photon energy fraction y (reconstructed experimentally from the Jacquet-Blondel variable y_{JB}) will be crucial for future comparisons.

Despite the large fluctuations of the data, one can say that there is a trend that theory overpredicts the data in the forward region. The reason might be that the isolation cut imposed at partonic level in the perturbative QCD calculation does not have the same effect as the experimental one. If the experimental cut is too stringent, a large fraction of the hadronic energy in the isolation cone may come from underlying events, such that experimentally a larger number of events is rejected. We gave a rough estimate of the underlying events to be expected in the isolation cone.

The possibilities offered by the study of photon + jet photoproduction will be investigated in a forthcoming publication [24].

Acknowledgements

We would like to thank P. Bussey from the ZEUS collaboration for helpful discussions. G.H. would like to thank the LAPTH for its continuous hospitality. This work was supported by the EU Fourth Training Programme "Training and Mobility of Researchers", network "Quantum Chromodynamics and the Deep Structure of Elementary Particles", contract FMRX-CT98-0194 (DG 12 - MIHT).

References

- [1] D. W. Duke and J. F. Owens, Phys. Rev. **D 26**, 1600 (1982).
- [2] P. Aurenche, A. Douiri, R. Baier, M. Fontannaz and D. Schiff, Z. Phys. **C24**, 309 (1984).
- [3] A. C. Bawa, M. Krawczyk and W. J. Stirling, Z. Phys. C **50**, 293 (1991).
- [4] P. Aurenche, P. Chiappetta, M. Fontannaz, J. Ph. Guillet and E. Pilon, Z. Phys. **C56**, 589 (1992).
- [5] L. E. Gordon and J. K. Storrow, Z. Phys. **C63**, 581 (1994).
- [6] L. E. Gordon and W. Vogelsang, Phys. Rev. **D 52**, 58 (1995).
- [7] L. E. Gordon, Phys. Rev. D **57**, 235 (1998).
- [8] M. Krawczyk and A. Zembrzusi, hep-ph/9810253.

- [9] R. K. Ellis and J. C. Sexton, Nucl. Phys. **B269**, 445 (1986).
- [10] P. Aurenche, R. Baier, A. Douiri, M. Fontannaz and D. Schiff, Nucl. Phys. **B286**, 553 (1987).
- [11] T. Binoth, J. Ph. Guillet, E. Pilon and M. Werlen, Eur. Phys. J. **C16**, 311 (2000).
- [12] P. Aurenche, L. Bourhis, M. Fontannaz and J. Ph. Guillet, Eur. Phys. J. **C17**, 413 (2000).
- [13] J. Breitweg *et al.* [ZEUS Collaboration], Phys. Lett. B **472**, 175 (2000).
- [14] P. Chiappetta, R. Fergani and J. Ph. Guillet, Z. Phys. **C69** 443 (1996).
- [15] M.A. Furman Nucl. Phys. **B197** 413 (1982);
W.T. Giele and E.W.N. Glover, Phys. Rev. **D46** 1980 (1992);
W.T. Giele, E.W.N. Glover and D. Kosower, Nucl. Phys. **B403** 633 (1993).
- [16] R.K. Ellis, D.A. Ross and A.E. Terrano, Nucl. Phys. **B187** 421 (1981);
S. Frixione, Z. Kunszt and A. Signer, Nucl. Phys. **B467** 399 (1996);
S. Catani and M.H. Seymour, Nucl. Phys. **B485** 291 (1997).
- [17] S. Frixione, Phys. Lett. **429B** 369 (1998).
- [18] P. Aurenche, F. W. Bopp, A. Capella, J. Kwiecinski, M. Maire, J. Ranft and J. Tran Thanh Van, Phys. Rev. D **45**, 92 (1992).
- [19] A. D. Martin, R. G. Roberts, W. J. Stirling and R. S. Thorne, Eur. Phys. J. C **14**, 133 (2000).
- [20] P. Aurenche, J. Ph. Guillet and M. Fontannaz, Z. Phys. C **64**, 621 (1994).
- [21] M. Glück, E. Reya and A. Vogt, Phys. Rev. D **45**, 3986 (1992).
- [22] L. Bourhis, M. Fontannaz and J. Ph. Guillet, Eur. Phys. J. C **2**, 529 (1998).
- [23] S. Kawabata, Comp. Phys. Comm. **88** 309 (1995).
- [24] M. Fontannaz, J. Ph. Guillet, G. Heinrich, in preparation.